

Developing correlation-consistent numeric atom-centered orbital basis sets for Krypton: Applications in RPA-based correlated calculations

Sixian Yang,^{1,2} Igor Ying Zhang,^{3,*} and Xinguo Ren^{2,†}

¹Key Laboratory of Quantum Information, University of Science and Technology of China, Hefei, 230026, China

²Institute of Physics, Chinese Academy of Sciences, Beijing 100190, China

³Collaborative Innovation Center of Chemistry for Energy Materials, Shanghai, Key Laboratory of Molecular Catalysis and Innovative Materials, MOE Key Laboratory of Computational Physical Sciences, Shanghai Key Laboratory of Bioactive Small Molecules, Department of Chemistry, Fudan University, Shanghai 200433, China

Localized atomic orbitals are the preferred basis-set choice for large-scale explicit correlated calculations, and high-quality hierarchical correlation-consistent basis sets are a prerequisite for correlated methods to deliver numerically reliable results. At present, Numeric Atom-centered Orbital (NAO) basis sets with valence correlation consistency (VCC), designated as NAO-VCC- nZ , are only available for light elements from hydrogen (H) to argon (Ar) (*New J. Phys.* **15**, 123033, (2013)). In this work, we extend this series by developing NAO-VCC- nZ basis sets for krypton (Kr), a prototypical element in the fourth row of periodic table. We demonstrate that NAO-VCC- nZ basis sets facilitate the convergence of electronic total-energy calculations using the Random Phase Approximation (RPA), which can be used together with a two-point extrapolation scheme to approach the complete-basis-set (CBS) limit. Notably, the Basis Set Superposition Error (BSSE) associated with the newly generated NAO basis sets is minimal, making them suitable for applications where BSSE correction is either cumbersome or impractical to do. After confirming the reliability of NAO basis sets for Kr, we proceed to calculate the Helmholtz free energy for Kr crystal at the theoretical level of RPA plus renormalized single excitation (rSE) correction. From this, we derive the pressure-volume (P - V) diagram, which shows excellent agreement with the latest experimental data. Our work demonstrates the capability of correlation-consistent NAO basis sets for heavy elements, paving the way toward numerically reliable correlated calculations for bulk materials.

I. INTRODUCTION

Kohn-Sham (KS) density functional theory (DFT) [1, 2] has become an indispensable tool for computational studies in physics, chemistry, and materials science. Practical applications of DFT rely on useful approximations to the exchange-correlation (XC) functional – the only unknown component in KS-DFT. The success of DFT lies largely in the fact that good compromise between accuracy and the computational cost can be achieved at the level of local and semi-local approximations [2–5]. Despite their success, these functionals suffer from intrinsic deficiencies, such as severe delocalization errors, the lack of long-range van der Waals interaction, and the incapability of dealing with strong electron correlations, to name a few [6]. To further improve the accuracy of first-principles approaches, recent advancements have focused on the development of so-called “fifth-rung” functionals. These include the Random Phase Approximation (RPA) [7–11] formulated within the adiabatic-connection fluctuation-dissipation theorem framework [12, 13], and doubly hybrid functionals [14–17] that integrate Density Functional Approximations

(DFAs) with explicit non-local correlated methods, such as the Møller–Plesset perturbation theory (MP2) [18].

One significant challenge associated with these fifth-rung functionals (and explicit correlated methods in general) is the need for a large amount of unoccupied single-particle orbitals. In practice, the corresponding correlation energy exhibits slow convergence with respect to the basis set size [9, 19–22]. This issue stems from the inadequate representation of the sharp Coulomb cusp at the electron-electron coordinate coalescence, where the first derivative of the many-electron wave function is discontinuous. Achieving an accurate description of such a cusp using smooth orbital expansions necessitates a large number of basis functions [23, 24]. Over the years, considerable efforts have been devoted to addressing the slow convergence of the electron correlation energy. One prevalent approach is the Complete Basis Set (CBS) extrapolation scheme [20, 21, 25–28], which is widely adopted by the quantum chemistry community to mitigate the Basis Set Incompleteness Errors (BSIE). This is accomplished by utilizing hierarchical basis sets allowing the convergence pattern of the correlation energy to be described through straightforward analytical formula. Another approach involves the utilization of explicit wave-function methods, such as the F_{12} method, [24, 29–31], which explicitly account for the electronic cusp and thereby reduce BSIE at finite basis sets.

Both techniques mentioned above have proven to be

* igor_zhangying@fudan.edu.cn

† renxg@iphy.ac.cn

successful for light elements and molecular systems. Gaussian-Type Orbitals (GTOs) are often the basis set choice for molecular calculations due to their nice analytical properties that facilitate the computation of multi-center integrals. In this regard, the correlation-consistent GTOs developed by Dunning [32], known as “cc-pVXZ” basis sets, have gained widespread acceptance in the field of quantum chemistry. Their systematic convergence behavior allows for reliable extrapolation to the CBS limit. In recent years, there has been considerable interest in applying quantum chemistry methods and fifth-rung functionals to extended periodic systems [33, 34]. In such cases, the standard cc-pVXZ basis sets, while effective for molecular calculations, are not optimal. One issue is that the extended tails of GTOs can result in an overlap matrix with a large condition number for extended periodic systems, rendering the preceding self-consistent calculations unstable before a sufficiently large GTO basis set can be employed for a reliable extrapolation. Secondly, the Basis Set Superposition Error (BSSE) associated with commonly used cc-pVXZ basis sets can be significant for correlation methods, which is difficult to correct in periodic systems. Within the quantum chemistry community, there is ongoing research aimed at developing GTOs better suited for correlated calculations in periodic systems. For example, Ye *et al.* [35] recently developed the “GTH-cc-pVXZ” GTOs, which are combined with the Goedecker-Teter-Hutter (GTH) type pseudopotentials [36, 37], to facilitate solid-state calculations using MP2 and Coupled Cluster theory at the level of Single, Double, and perturbative Triple excitations (CCSD(T)).

Alternatively, plane-wave basis sets can be used for correlated calculations in solid-state systems [38, 39]. However, it should be noted that the pseudopotentials designed for ground-state DFAs may not be suitable for such correlated calculations. For example, special pseudopotentials must be developed for high-precision *GW* calculations in the projector augmented wave framework [40]. Furthermore, plane-wave basis sets make it challenging to formulate low-scaling algorithms that fully exploit Kohn’s nearsightedness principle [41]. Although $O(N^3)$ -scaling algorithm has been developed for RPA and *GW* utilizing the fast Fourier transform between real and reciprocal space [42] and the efficient Fourier transform between the imaginary time and frequency domains [43], further scaling reductions that make use of the intrinsic locality of the electronic structure have not yet been reported.

In the case of Numeric Atom-centered Orbitals (NAOs), the situation is even less satisfactory. In 2013, Zhang *et al.* developed the valence-correlation-consistent NAO basis sets, termed as NAO-VCC- nZ [44], which are apt for correlated calculations in molecular calculations. However, NAO-VCC- nZ is currently only available for light elements from H to Ar. For solid-state calculations, these basis sets require further refinement and modification to alleviate the ill-conditioning problem [45], which

is more pronounced in solids compared to molecules when using large basis sets. Consequently, there is an urgent need to develop correlation-consistent NAO basis sets that are 1) applicable to heavier elements beyond Ar, and 2) suitable for solid-state calculations.

In this work, we first construct hierarchical valence-correlation-consistent NAO basis sets for the element krypton (Kr), largely adhering to the prescription developed in Ref. [44]. Specifically, the basis functions are generated by minimizing the frozen-core PBE-based RPA total energy for a single atom, while subject to the “eventempered” principle, akin to the approach used in the construction of cc-pVXZ basis sets. The candidate basis functions are all “hydrogen-like” functions [46]. We then assess the performance of the newly generated NAO-VCC- nZ ($n=2-5$) basis sets for both Kr dimer (Kr_2) and Kr crystal systems. Systematic convergence behaviors of the binding energies are observed for both the dimer and bulk systems, allowing for reliable extrapolation to the CBS limit. More importantly, our comparison with and without counterpoise corrections reveals that these new NAO basis sets carry rather small BSSE, permitting reliable calculations even without BSSE corrections. In contrast, the cc-pVXZ GTOs and FHI-aims-2009 (*tier*’s) NAOs for Kr are contaminated with huge BSSE, resulting in the binding energies that necessitate BSSE corrections for obtaining meaningful results. The minimal and controllable BSSE in the newly generated NAO-VCC- nZ for Kr offers a significant advantage, especially in situations where BSSE corrections are cumbersome or impractical to perform. Finally, we calculate the Helmholtz free energy of the face-centered-cubic (FCC) Kr crystal, based on which the P - V curve at finite temperatures can be attained. The electronic part of the free energy is obtained from converged RPA+rSE calculations. The final RPA+rSE based P - V curve shows excellent agreement with experimental measurements for compressed Kr crystal across a broad pressure range. The experience gained from developing these correlation-consistent NAO basis sets for Kr is highly useful for guiding similar efforts for other heavy elements. Works on constructing correlation-consistent NAO basis sets for other fourth-row elements are still ongoing, and will be published elsewhere.

The paper is organized as follows. Sec. II outlines the fundamentals of NAO basis sets, focusing on the prescription used to generate correlation-consistent NAOs for Kr, along with the computational details of the present work. The major results are presented in Sec. III, including the detailed layout of the NAO-VCC- nZ basis sets for Kr (Sec. III A), a systematic study of the convergence behavior of the new basis sets for both Kr_2 and the bulk system (Sec. III B), and the P - V curve based on converged RPA+rSE calculations (Sec. III C). The paper concludes in Sec. IV.

II. METHODOLOGY AND COMPUTATIONAL DETAILS

A. Numerical atomic-centered basis sets

In this work, all calculations are performed using the *all-electron* Fritz Haber Institute *ab initio* molecular simulations (FHI-aims) code package [46]. The primary basis-set choice of FHI-aims is NAO $\{\phi_i(\mathbf{r})\}$, given by numerically tabulated radial functions multiplied by real spherical harmonics,

$$\phi_i(\mathbf{r}) = \frac{u_i(r)}{r} Y_{lm}(\Omega), \quad (1)$$

where $Y_{lm}(\Omega)$ denotes real parts ($m = 0, \dots, l$) and imaginary parts ($m = -l, \dots, -1$) of complex spherical harmonics. In FHI-aims, one has the flexibility to use radial functions with analytic forms, such as Slater-Type Orbitals (STOs) or GTOs. Generally, the radial part of the NAOs $u_i(r)$ is obtained by solving the following radial Schrödinger equation,

$$\left[-\frac{1}{2} \frac{d^2}{dr^2} + \frac{l(l+1)}{2r^2} + v_i(r) + v_{cut}(r) \right] u_i(r) = \epsilon_i u_i(r). \quad (2)$$

In Eq. 2, the total effective potential contains two parts: a radial potential $v_i(r)$, which governs the main shape of $u_i(r)$, and a confining potential $v_{cut}(r)$ which is switched on beyond a certain distance r_{onset} from the nucleus and becomes infinite at $r_{onset} + w$. Careful tests indicate that $w = 2.0 \text{ \AA}$ is a good default value, which ensures a smooth decay of the radial tails of $u_i(r)$ to strict zero at $r_{onset} + w$. The choice of the cutoff radius r_{onset} of the confining potential $v_{cut}(r)$ has been tested by Zhang *et al.* [44] and it was shown that the energy variation is at the level of meV for r_{onset} changes from 4.0 to 6.0 \AA . This uncertainty is negligible compared to the typical BSIE for correlation methods [9].

In FHI-aims, NAO basis sets feature the use of so-called “minimal basis functions”, which are generated from self-consistent, non-spin-polarized, and spherically symmetric free-atom radial potential $v_i(r) = v_{at}^{free}(r)$. The minimal basis consists of core and valence functions for all occupied states, exhibiting excellent performance by naturally capturing wavefunction oscillations near the nucleus, where the nuclear Z/r potential dominates. Hence the minimal basis serves as a natural foundation for constructing NAO basis sets for correlated methods. Also, it is worth noting that the description of the minimal basis of NAOs requires less dense radial grids for light elements compared to GTOs such as Dunning’s cc-pVXZ basis, as demonstrated in Ref. [47].

B. NAO-VCC- nZ basis sets with valence correlation consistency

Currently, there exists a set of optimized NAO basis sets, referred to as FHI-aims-2009 or more commonly as “*tier- n* ” basis sets [46], which are the standard choice for the ground-state calculations in FHI-aims. FHI-aims-2009 basis sets are constructed by a step-wise minimization of total energy from LDA calculations of selected dimers. Studies employing *tier- n* basis sets for conventional (semi)-local and hybrid DFAs have demonstrated their high efficacy [10, 46]. However, reliable results for correlation methods that require virtual states can only be achieved when a counterpoise (CP) correction is applied. In 2013, a new sequence of NAO basis sets, inspired by Dunning’s correlation-consistency strategy, was developed [47]. These NAO basis sets, designated as “NAO-VCC- nZ ”, achieve systematic convergence of the frozen-core RPA total energy to the CBS limit. More importantly, a two-point extrapolation to the CBS limit effectively mitigates the BSSE issue, which is important in situations where a CP correction is impractical. Unfortunately, these NAO-VCC- nZ basis sets are currently limited to light elements from H to Ar.

In this work, we extend the work of Ref. [44, 45] to construct the NAO-VCC- nZ basis sets for a prototypical fourth-row main-group element – Kr. We group our NAO basis into “one base + two subsets”, where “one base” refers to the minimal basis described above, and the “two subsets” include: i) the (*sp*) correlation set, ii) the polarization set on top of the FHI-aims original minimal basis. Here, (*sp*) indicates that only *s*- and *p*-type orbitals are used, and the polarization set includes NAOs with higher momenta, i.e. *d*, *f*, *g* functions, etc. The $4s^2 4p^6$ valence-shell configuration is adopted for Kr in post-KS RPA calculations, while occupied $3d$ and lower states are frozen. We employ radial functions $u_i(r)$ generated via hydrogen-like radial potential $v_i(r) = z_i/r$ for all angular momenta l , and each radial function yields $2l + 1$ basis functions by multiplying the real spherical harmonics (cf. Eq. 1). Here we set the principal quantum number $n = l + 1$, resulting in nodeless radial functions similar to STOs [48, 49].

The effective nuclear charge $\{z_i\}$, which determines the actual shape of hydrogen-like basis functions, is the major parameter to be optimized. For those nodeless radial functions, we use “even-tempered” [50] scheme to expand the effective nuclear charges:

$$z_i = \alpha \beta^{i-1} \quad i = 1, 2, \dots, N_{orb}. \quad (3)$$

Here the nuclear charges $\{z_i\}$ are represented by two parameters (α, β) which are the actual parameters to be optimized. Individual subsets of radial functions with the same angular momentum l share the same (α, β) parameters. For example, in the case of a quadruple- ζ basis one could expand all three *s*-type functions via the optimization of a pair of parameters (α_1, β_1) , while a new

pair of parameters (α_2, β_2) should be used for three d -type functions in the polarization set, and so on.

Following Ref. [47], we chose the frozen-core RPA@PBE energy of a single Kr atom as the optimization target for the parameters characterizing the basis functions. Our optimization procedure proceeds as follows: Initially, the sp correlation subset is optimized, followed by the optimization of the polarization subset. Subsequently, the sp correlation subset undergoes a re-optimization as the final step. The Nealder-Mead downhill simplex algorithm [51] is used for executing the optimization of the parameters (α, β) , with a convergence criterion of 10^{-3} for the effective nuclear charge Z . This corresponds to an approximate convergence criterion of 10^{-6} eV for the RPA total energy. To search for the global minimum, we explored various initial guesses for (α, β) within a reasonable window, using a tabulated grid.

C. Computational details

The total energy of RPA as a post-KS computational method is given by

$$E^{\text{RPA}} = E^{\text{DFA}} - E_{xc}^{\text{DFA}} + E_x^{\text{EX}} + E_c^{\text{RPA}}, \quad (4)$$

whereby the XC component E_{xc}^{DFA} of the total energy of a conventional DFA, E^{DFA} , is replaced by the exact-exchange energy E_x^{EX} plus RPA correlation energy E_c^{RPA} , both evaluated in terms of pre-determined DFA orbitals and orbital energies. Furthermore, a ‘‘single excitation’’ (SE) term, and in particular its renormalized version (termed as renormalized SE, or rSE) E_c^{rSE} can be added to the standard RPA total energy to alleviate the under-binding behavior of RPA for molecules and solids. This correction scheme has been discussed in Refs. [11, 52], and subsequently in Ref. [40]. Benchmark tests for NAO-based RPA and RPA+rSE calculations have demonstrated the excellent performance of these computational schemes for accurately describing both molecular and periodic systems [10, 11, 45, 53, 54].

The employment of NAO-VCC- nZ basis sets allows the RPA or RPA+rSE total energy to be extrapolated to the CBS limit via the following formula [55, 56],

$$E(n) = E(\infty) - C/n^3. \quad (5)$$

In Eq. 5, n is the cardinal number of the NAO-VCC- nZ basis sets, and C is a fitting parameter. Equation 5 is a widely used two-point extrapolation formula initially developed for correlation-consistent Gaussian basis sets [56], but also works well for NAO-VCC- nZ basis sets [44]. In this work, basis sets with $n=4, 5$ are used for the extrapolation, implying that

$$E(\infty) = \frac{E(4)4^3 - E(5)5^3}{4^3 - 5^3}. \quad (6)$$

The CBS limit results obtained via Eq. 6 are denoted as CBS(4,5). Conventional DFAs that require only occupied states converge much faster with respect to the basis set size. In this work, a finite NAO-VCC-5Z basis set is used for conventional DFA calculations, which proves to be adequate. Also, for periodic systems, a finite \mathbf{k} -point mesh is used for Brillouin-zone sampling. For FCC primitive cell, an $8 \times 8 \times 8$ \mathbf{k} grid is used, which is sufficient to achieve sub-meV precision for the RPA total energy. Moreover, the scaled zeroth-order regular approximation (ZORA) [57] scheme is employed to account for the relativistic effect.

For free energy calculations, one needs to take into account of the entropy contribution from lattice vibrations. In this work, we calculate the phonon spectra at the PBE level, and the Helmholtz free energy at a given volume V and temperature T invoked to determine the P - V diagram is given as

$$F(V, T) = E^{\text{RPA+rSE}}(V) + \frac{1}{2} \sum_{\mathbf{q}, j} \hbar \omega_{\mathbf{q}, j}(V) + k_B T \sum_{\mathbf{q}, j} \ln \left[2 \sinh \left(\frac{\hbar \omega_{\mathbf{q}, j}(V)}{2k_B T} \right) \right] \quad (7)$$

Here the summation over \mathbf{q} goes over the Brillouin zone and j labels different phonon modes. Furthermore, in Eq. 7 $E^{\text{RPA+rSE}}(V)$ is the RPA+rSE total energy at 0 K, and the second and third terms correspond to the contributions from zero-point energies and lattice vibrations at finite temperatures. The phonon frequencies are calculated by the finite displacement method as implemented in the PHONOPY code [58] interfaced with FHI-aims. Convergence criteria for the total energy and force are set to 10^{-6} eV and 10^{-5} eV/Å, respectively. A displacement of 0.002 Å for the finite displacement method is adopted. In Ref. [53], the influence of the employed functionals on the phonon spectrum and the subsequent free energy calculations was investigated, the conclusion was that the use of PBE functional instead of the RPA+rSE in the phonon calculations should be adequate for calculating the P - V curve.

III. RESULTS AND DISCUSSIONS

A. NAO-VCC- nZ basis sets of Kr

As discussed in Sec. IIB, each of the NAO-VCC- nZ basis sets for Kr consists of a subset of sp correlation functions, a subset of polarization functions, and a base of minimal basis functions. The former two subsets are optimized in this work, and the layouts of these two subsets for $n = 2, 3, 4, 5$ are shown in Table I. In addition, the same minimal basis functions of ($4s$ $3p$ $1d$) for Kr are included in all NAO-VCC basis sets and added up in total count in Table I. Note that the minimal basis functions are determined using Eq. 2 and hence their exact

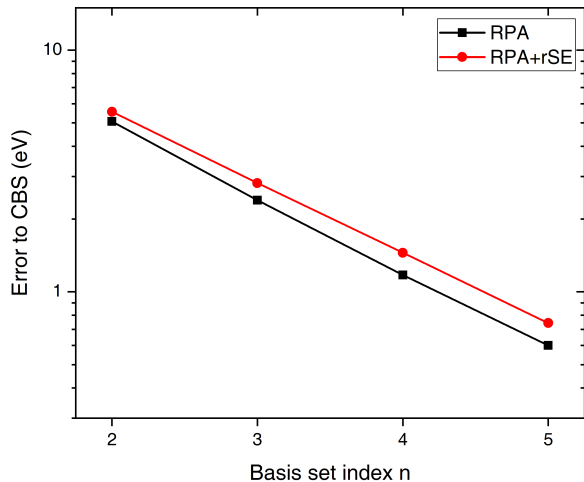


FIG. 1. Basis set errors of the RPA@PBE and (RPA+rSE)@PBE correlation energies for isolated Kr atom. The CBS(4,5) results are taken as the references.

shape will (slightly) depend on the actual XC potential used in the SCF calculations.

Similar to the Dunning’s cc-pVXZ basis sets [32] and the NAO-VCC- n basis sets for light elements [47], the newly generated NAO-VCC- n Z basis sets for Kr adhere to the “correlation consistency” principle. Specifically, the increase of the correlation energy resulting from the inclusion of the n -th polarization function with angular momentum l is approximately equal to the increase stemming from the inclusion of the $(n-1)$ -th polarization function with angular momentum $l+1$. As illustrated in Fig. 1, the RPA and RPA+rSE correlation energies for the Kr atom exhibit a clear exponential convergence as a function of the basis set index n . In Table. S1 of the Supplementary Materials (SM), the parameter settings of the NAO-VCC- n Z basis sets for Kr as used in FHI-aims calculations are presented.

B. Binding energy curves of the Kr dimer and solid bulk

We now examine the performance of NAO-VCC- n Z basis sets on calculating the binding energies of the Kr dimer – Kr₂. Figure 2 presents the (RPA+rSE)@PBE binding energy curves for Kr₂, which are calculated using NAO-VCC- n Z with $n = 2$ to 5, as well as the extrapolated CBS(4,5) limit. The left and right panels of Fig. 2 show the results without and with CP corrections, respectively. Additionally, we performed RPA+rSE calculations using Gaussian cc-pV5Z and FHI-aims-2009 NAO basis sets for comparative analysis. For the latter, we choose *tier 2* plus some additional functions (denoted here as “*tier2+*”). It is the largest basis set of this type available for Kr. To isolate the impact of basis-set errors, a very tight convergence criterion is applied to numeri-

cal integration in both radial and angular parts. The calculated equilibrium bond lengths and the corresponding binding energies for various basis sets are listed in Table II.

Figure 2 shows that the newly generated NAO-VCC- n Z basis sets for Kr yield systematically converging RPA+rSE binding energies for the Kr₂. More importantly, a comparison between the left and right panels of Fig. 2 reveals that the BSSEs associated with NAO-VCC- n Z are rather small, corresponding to a small fraction of the total binding energy. In stark contrast, binding energies calculated using cc-pV5Z and the NAO *tier2+* basis sets are contaminated with substantial BSSE. Without performing CP corrections, both cc-pV5Z and *tier2+* significantly overestimate the binding energies by an order of magnitude, rendering the results entirely unusable. These discrepancies are evident in both Fig. 2 and Table II. Further results for other cc-pVXZ basis sets are presented in Fig. S1 of the SM.

It should be noted that, by introducing an augmented set of diffuse functions, aug-cc-pVXZ basis sets usually outperform cc-pVXZ, in particular for weak interactions [47]. However, unlike aug-cc-pVXZ basis sets, our NAO-VCC- n Z basis sets do not incorporate an augmented set of diffuse functions. As shown in Fig. S2 in the SM, the introduction of diffuse functions to NAO-VCC-5Z leads to a CP-corrected bonding energy of -13.70 meV, which is similar to the NAO-VCC-5Z result without CP corrections (-12.37 meV, see Table II). This is appealing since in many situations it is too cumbersome or impractical to perform BSSE corrections, and in such situations the newly generated NAO-VCC- n Z basis set for Kr can be directly used, expecting that the small and controllable BSSE of this basis set compensates the effect of missing diffuse functions.

Next, we examine the performance of NAO-VCC- n Z basis sets in calculating cohesive energies using RPA-type methods for bulk systems. Figure 3 presents the cohesive energy curves for Kr FCC crystal based on RPA (left side) and RPA+rSE (right side) methods using NAO-VCC- n Z basis sets with $n=2-5$. As before, the figure also includes the extrapolated CBS(4,5) results. A consistent convergence pattern relative to the cardinal number n is again observed. However, it’s worth noting that for bulk Kr, the results obtained using 2Z or 3Z basis sets are still quite far from the CBS limit. Therefore, extrapolation based on larger basis sets, such as 4Z and 5Z, is necessary. Furthermore, a comparison between the left and right sides of Fig. 3 reveals that the rSE correction significantly enhances the binding strength. Concretely, RPA tends to underbind, while RPA+rSE tends to overbind the Kr crystal, respectively.

In Fig. 4, we present the cohesive energies of the FCC Kr crystal as a function of the lattice constant calculated using RPA@PBE and (RPA+rSE)@PBE. For comparison, we also include results of lower-rung functionals, including LDA, GGA-PBE, the global hybrid functional PBE0 [62], the Heyd-Scuseria-Ernzerhof (HSE) screened

TABLE I. Number of radial functions in Kr NAO-VCC- nZ ($n=2,3,4,5$) basis sets. The minimal basis set of $(4s\ 3p\ 1d)$ is not shown in this table, but is added up in the total count.

	(sp) correlation subset	polarization subset	total
NAO-VCC-2Z	$(1s\ 1p)$	$(1d)$	$(5s\ 4p\ 2d)$
NAO-VCC-3Z	$(2s\ 2p)$	$(2d\ 1f)$	$(6s\ 5p\ 3d\ 1f)$
NAO-VCC-4Z	$(3s\ 3p)$	$(3d\ 2f\ 1g)$	$(7s\ 6p\ 4d\ 2f\ 1g)$
NAO-VCC-5Z	$(4s\ 4p)$	$(4d\ 3f\ 2g\ 1h)$	$(8s\ 7p\ 5d\ 3f\ 2g\ 1h)$

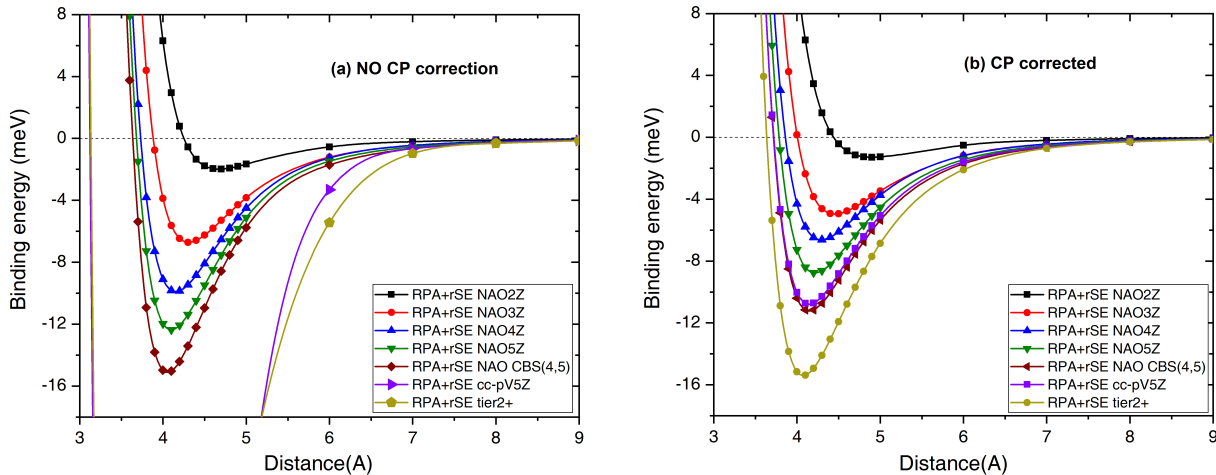


FIG. 2. Binding energy curves of Kr_2 without CP correction (left panel) and with CP correction (right panel) are shown. NAO-VCC- nZ basis set is extrapolated to CBS limit CBS(4,5) and the other basis sets are using the largest size of its family (e.g. *tier2+*, *cc-pV5Z*).

hybrid functional [63], as well as PBE complemented with vdW(TS) [64] and with the many-body dispersion (MBD) [65]. The experimental equilibrium lattice constant and cohesive energy are marked by dashed lines in the figure. Here the reference cohesive energy has been corrected for zero-point vibration energies as determined by accurate quantum chemical methods [61]. Similar to other noble-gas crystals, an accurate description of the cohesive properties of the Kr crystal is challenging for conventional DFAs. LDA and PBE exhibit substantial overbinding and underbinding tendencies, respectively. Hybrid functionals like PBE0 or HSE offer no improvement over PBE, due to their inability to capture long-range vdW interactions. Conventional GGA-PBE combined with semi-empirical vdW corrections, like PBE+vdW(TS) and PBE+MBD, improves accuracy for weak interactions but still underestimates the cohesive energy and overestimates the equilibrium lattice constant.

Regarding the performance of RPA, we obtained an equilibrium lattice constant of 5.770 \AA and a cohesive energy of -101.7 meV at the CBS(4,5) level. Compared to the experimental data of 5.670 \AA and -121.8 meV [60], the standard RPA@PBE scheme exhibits a noticeable underbinding, despite its significant improvement over conven-

tional DFAs. This underbinding tendency of RPA has also been observed by Klimeš *et al.* [40], based on plane-wave-based RPA implementation [66]. As previously discussed, RPA@PBE typically underbinds molecules and solids due to overestimated Pauli repulsion, which can be largely corrected by adding single-excitation corrections [11, 40, 52]. Figure 4 shows that incorporating the rSE correction enhances the cohesive energies of the Kr crystal, resulting in an equilibrium lattice constant of 5.633 \AA and a cohesive energy of -136.3 meV . While this is generally satisfactory, an overestimation of cohesive energy by 14 meV is noticeable, which can be partly attributed to the lack of BSSE correction in the bulk calculations. Table. S2 of the SM indicates that, with the CP correction, the binding energies are reduced by about 24 meV , leading to a BSSE-corrected RPA+rSE binding energy of -112.1 meV . It is worth pointing out that this value is close to the NAO-VCC-5Z result (see Fig 4), indicating a compensation between the small BSSE and the BSIE in the finite basis set. The fully numerically converged RPA+rSE cohesive energy for Kr FCC crystal is most likely in between the CP-corrected and uncorrected values, aligning well with the experimental result.

TABLE II. Equilibrium bond lengths r_e (in Å) and interaction energies D_e (in meV) of RPA+rSE obtained using various different basis sets. Results obtained both with (right side) and without (left side) CP corrections are presented.

Basis set	no CP correction		CP corrected	
	r_e	D_e	r_e	D_e
NAO-VCC-3Z	4.31	-6.71	4.46	-4.96
NAO-VCC-4Z	4.15	-9.90	4.29	-6.63
NAO-VCC-5Z	4.10	-12.37	4.21	-8.76
NAO-VCC CBS(4,5)	4.05	-15.12	4.15	-11.22
<i>tier2+</i>	3.58	-90.92	4.08	-15.39
cc-pV5Z	3.69	-121.53	4.15	-10.79

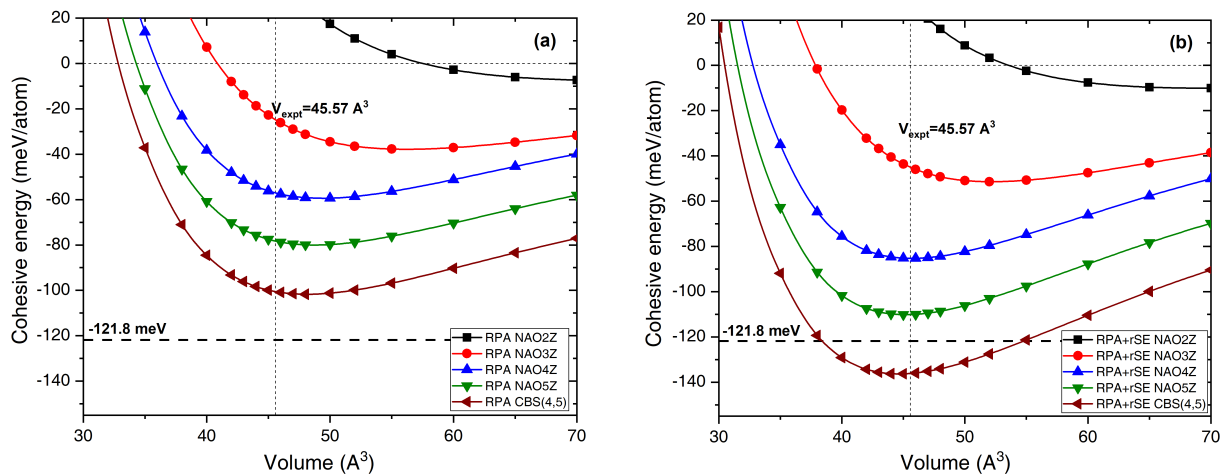


FIG. 3. Fitting curve under second-order Birch–Murnaghan equation of state method for the FCC Kr crystal. The experimental cohesive energy corrected by zero-point vibration energy from accurate CCSD(T) is shown as black dashed line, -121.8 meV.

C. P - V curve of Kr FCC crystal in the high-pressure regime

The study of matter under high pressure is an important area of research in condensed-matter physics, as a plethora of intriguing phenomena might emerge in this regime. Fascinating structural transition or abrupt changes in conductivity and other electronic-structure-derived properties are often observed in experiments. For example, it has been shown that the application of high pressure can induce a phase transition from tri-layer graphene to hexagonal diamond structure [67], and a structural transformation from $2H_c$ to $2H_a$ in MoS_2 [68]. At ultrahigh pressure, superconductivity has even been observed in pristine $2H_a$ - MoS_2 [69]. Similar phenomena have been reported in the family of rare-gas solids. Specifically, a FCC-HCP phase transition has been experimentally observed [70–74], accompanied by changes in the band structure [75, 76]. More recently, it was found that Kr may exhibit significant stacking disorders in its FCC lattice. Furthermore, the FCC and HCP phases have been found to coexist over a wide pres-

sure range from 2.7 to 140 GPa upon high-temperature annealing via laser heating [77]. While considerable theoretical efforts have been devoted to the understanding of the physical properties of rare gas systems under high pressure [78–81], a quantitative description achieving experimental accuracy remains a significant challenge.

Having verified the reliability of our NAO-VCC- n Z basis set for Kr and the good performance of the RPA+rSE method in describing the cohesive property of the Kr crystal, we set out to determine the P - V diagram theoretically. To achieve this, we calculate the Helmholtz free energy $F(V, T)$ according to Eq 7. Subsequently, we determine the pressure at a given temperature and volume via $P(V, T) = -\partial F(V, T)/\partial V|_T$, which allows us to generate the P - V curves at various temperatures. In Fig. 5, we present the calculated (RPA+rSE)@PBE and PBE P - V curves at $T = 300$ K for the FCC phase of Kr crystal. Furthermore, we include four sets of experimental data for comparative analysis.

Figure 5 shows that our calculated RPA+rSE P - V curve is in overall good agreement with the experimental results of Polian *et al.* [82] and Jephcoat *et al.* [83] extracted from energy-dispersive x-ray diffraction data,

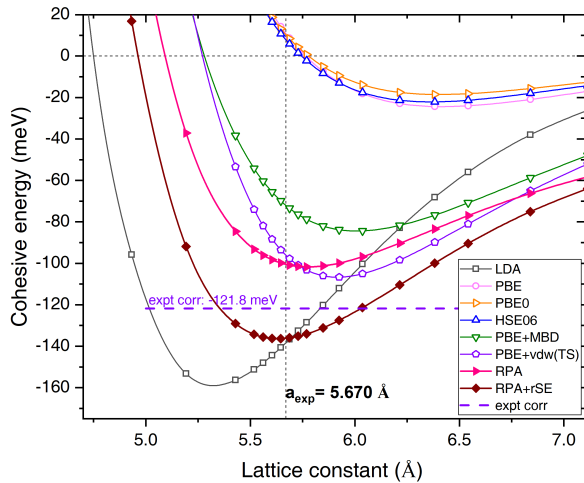


FIG. 4. Cohesive energies of the FCC Kr crystal determined by different functionals. The RPA and RPA+rSE results are obtained by extrapolating the NAO-VCC-4Z and 5Z results to the complete basis set (CBS) limit, and all other results are obtained using the NAO-VCC-5Z basis set. A FCC primitive unit cell and $8 \times 8 \times 8$ k grid sampling are used in all calculations. Experimental values are corrected with zero-point vibration energies by accurate quantum chemical method from reference [59–61].

and those of Errandonea *et al.* [73] and Rosa *et al.* [77] extracted from *in-situ* x-ray diffraction and absorption measurements. Note that, there are noticeable discrepancies among the various sets of experimental data themselves. Here, we focus on the comparison to the experimental data from Rosa *et al.*, as it represents the most recent and comprehensive investigation of Kr under high-pressure conditions, extending up to 140 GPa. Overall our theoretical P - V curve agrees well with the experimental data of Rosa *et al.* in both high and low pressure regimes. For comparison, we also include the calculated PBE P - V curve in Fig. 5. It is evident that the PBE method tends to overestimate the pressure (i.e., a higher pressure is needed to compress the Kr crystal to the same volume), a tendency that is pronounced in the low and medium pressure range.

IV. CONCLUSION

In this work, we developed valence-correlation-consistent NAO basis sets for the Kr element. Our tests on the binding energies of Kr_2 and the cohesive energies of Kr FCC crystal demonstrate that these basis sets yield systematic convergence patterns for RPA-type correlated calculations. This allows for a reliable extrapolation to the CBS limit. More importantly, these newly generated NAO-VCC- n Z basis sets for Kr exhibit minimal BSSE, in stark contrast with the Gaussian cc-pVXZ

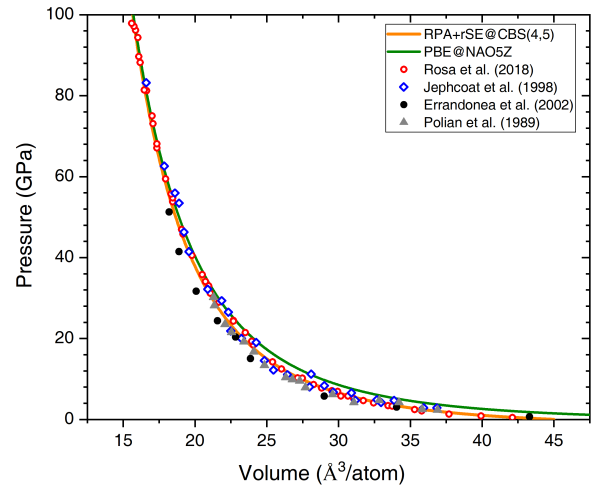


FIG. 5. Calculated P - V diagram at 300 K for the FCC phase of the Kr crystal. The results are extrapolated to the CBS limit [CBS(4,5)]. The electronic part of the free energy is obtained using RPA+rSE, complemented with PBE phonon free energy at 300 K (orange line). Reference data from four experimental studies are included for comparison.

basis sets and the FHI-aims-2009 NAO basis sets. This feature makes them particularly useful in the correlated calculations of extended materials, where a CP correction for BSSE is often impractical. We then calculated the Helmholtz free energy and derived the P - V curve for the FCC phase of the Kr crystal, based on converged RPA+rSE calculations for the electronic part of the free energy. The resulting theoretical P - V curve is in excellent agreement with the most recent experiment data. The insights and methodologies developed in this study offer valuable guidance for constructing NAO-VCC basis sets for other heavy elements. Overall, our research investigates the capability of correlation-consistent NAO basis sets for heavy elements, laying the groundwork for conducting reliable correlated calculations at the RPA level and beyond in extended materials.

ACKNOWLEDGMENTS

The work is supported by the National Key R & D Program of China (Grant No. 2022YFA1403800) and the National Natural Science Foundation of China (Grant Nos. 12188101, 12134012, 21973015, and 22125301), as well as by the Max Planck Partner Group for *Advanced Electronic Structure Methods*, and innovative research team of high-level local universities in Shanghai and a key laboratory program of the Education Commission of Shanghai Municipality (ZDSYS14005).

ADDITIONAL INFORMATION

Competing interest: The authors declare no competing financial or non-financial interests.

DATA AVAILABILITY

All the input and output files of the calculations involved in this work have been uploaded to the NO-

MAD repository and can be found under the link <https://dx.doi.org/10.17172/NOMAD/2023.09.01-1>.

-
- [1] P. Hohenberg and W. Kohn, *Phys. Rev.* **136**, B864 (1964).
- [2] W. Kohn and L. J. Sham, *Phys. Rev.* **140**, A1133 (1965).
- [3] J. P. Perdew and A. Zunger, Self-Interaction Correction to Density-Functional Approximation for Many-Electron Systems, *Phys. Rev. B* **23**, 5048 (1981).
- [4] J. P. Perdew, K. Burke, and M. Ernzerhof, Generalized Gradient Approximation Made Simple, *Phys. Rev. Lett.* **77**, 3865 (1996).
- [5] J. Sun, A. Ruzsinszky, and J. P. Perdew, Strongly constrained and appropriately normed semilocal density functional, *Phys. Rev. Lett.* **115**, 036402 (2015).
- [6] A. J. Cohen, P. Mori-Sánchez, and W. Yang, Challenges for Density Functional Theory, *Chemical Reviews* **112**, 289 (2012), pMID: 22191548, <https://doi.org/10.1021/cr200107z>.
- [7] D. Bohm and D. Pines, A Collective Description of Electron Interactions: III. Coulomb Interaction in a Degenerate Electron Gas, *Phys. Rev.* **92**, 609 (1953).
- [8] H. Eshuis, J. E. Bates, and F. Furche, Electron Correlation Methods Based on the Random Phase Approximation, *Theor. Chem. Acc.* **131**, 1084 (2012).
- [9] X. Ren, P. Rinke, C. Joas, and M. Scheffler, Random-phase approximation and its applications in computational chemistry and materials science, *J. Mater. Sci.* **47**, 7447 (2012).
- [10] X. Ren, P. Rinke, V. Blum, J. Wieferink, A. Tkatchenko, A. Sanfilippo, K. Reuter, and M. Scheffler, *New J. Phys.* **14**, 053020 (2012).
- [11] X. Ren, P. Rinke, G. E. Scuseria, and M. Scheffler, Renormalized second-order perturbation theory for the electron correlation energy: Concept, implementation, and benchmarks, *Phys. Rev. B* **88**, 035120 (2013).
- [12] D. C. Langreth and J. P. Perdew, Exchange-correlation energy of a metal surface: Wave-vector analysis, *Phys. Rev. B* **15**, 2884 (1977).
- [13] O. Gunnarsson and B. I. Lundqvist, Exchange and correlation in atoms, molecules, and solids by the spin-density-functional formalism, *Phys. Rev. B* **13**, 4274 (1976).
- [14] Y. Zhao, B. J. Lynch, and D. G. Truhlar, Development and Assessment of a New Hybrid Density Functional Model for Thermochemical Kinetics, *J. Phys. Chem. A* **108**, 2715 (2004).
- [15] S. Grimme, Semiempirical hybrid density functional with perturbative second-order correlation, *J. Chem. Phys.* **124**, 034108 (2006).
- [16] Y. Zhang, X. Xu, and W. A. Goddard III, Doubly hybrid density functional for accurate descriptions of nonbond interactions, thermochemistry, and thermochemical kinetics, *Proc. Nat. Acad. Sci. U. S. A.* **106**, 4963 (2009).
- [17] I. Y. Zhang and X. Xu, *A New-Generation Density Functional* (Springer, New York, 2014).
- [18] C. Møller and M. S. Plesset, *Phys. Rev.* **46**, 618 (1934).
- [19] S. Lebègue, J. Harl, T. Gould, J. G. Ángyán, G. Kresse, and J. F. Dobson, Cohesive Properties and Asymptotics of the Dispersion Interaction in Graphite by the Random Phase Approximation, *Phys. Rev. Lett.* **105**, 196401 (2010).
- [20] J. Harl, L. Schimka, and G. Kresse, Assessing the quality of the random phase approximation for lattice constants and atomization energies of solids, *Phys. Rev. B* **81**, 115126 (2010).
- [21] H. Eshuis and F. Furche, Basis set convergence of molecular correlation energy differences with the random phase approximation, *J. Chem. Phys.* **136**, 084105 (2012).
- [22] B. G. Janesko, T. M. Henderson, and G. E. Scuseria, Long-range-corrected hybrids including random phase approximation correlation, *J. Chem. Phys.* **130**, 081105 (2009).
- [23] D. P. Tew, W. Klopper, and T. Helgaker, Electron correlation: The many-body problem at the heart of chemistry, *Journal of computational chemistry* **28**, 1307 (2007).
- [24] J. Noga, W. Kutzelnigg, and W. Klopper, CC-R12, a correlation cusp corrected coupled-cluster method with a pilot application to the Be₂ potential curve, *Chemical physics letters* **199**, 497 (1992).
- [25] A. Grüneis, M. Marsman, J. Harl, L. Schimka, and G. Kresse, Making the random phase approximation to electronic correlation accurate, *J. Chem. Phys.* **131**, 154115 (2009).
- [26] F. Furche, Molecular tests of the random phase approximation to the exchange-correlation energy functional, *Phys. Rev. B* **64**, 195120 (2001).
- [27] E. Fabiano and F. Dalla Sala, Accuracy of basis-set extrapolation schemes for DFT-RPA correlation energies in molecular calculations, *Theor. Chem. Acc.* **131**, 1278 (2012).
- [28] A. Grüneis, M. Marsman, and G. Kresse, Second-order Møller–Plesset perturbation theory applied to extended systems. II. Structural and energetic properties, *J. Chem. Phys.* **133**, 074107 (2010).
- [29] G. Hattig, W. Klopper, A. Kohn, and D. P. Tew, Explicitly correlated electrons in molecules, *Chemical reviews* **112**, 4 (2012).

- [30] L. Kong, F. A. Bischoff, and E. F. Valeev, Explicitly correlated R12/F12 methods for electronic structure, *Chemical reviews* **112**, 75 (2012).
- [31] W. Kutzelnigg and W. Klopper, Wave functions with terms linear in the interelectronic coordinates to take care of the correlation cusp. I. General theory, *J. Chem. Phys.* **94**, 1985 (1991).
- [32] J. T. H. Dunning, Gaussian basis sets for use in correlated molecular calculations. I. The atoms boron through neon and hydrogen, *J. Chem. Phys.* **90**, 1007 (1989).
- [33] Y. Wang, Y. Li, J. Chen, I. Y. Zhang, and X. Xu, Doubly Hybrid Functionals Close to Chemical Accuracy for Both Finite and Extended Systems: Implementation and Test of XYG3 and XYGJ-OS, *JACS Au* **1**, 543 (2021), publisher: American Chemical Society.
- [34] I. Y. Zhang and A. Grüneis, Coupled Cluster Theory in Materials Science, *Front. Mater.* **6**, Article 123 (2019).
- [35] H.-Z. Ye and T. C. Berkelbach, Correlation-consistent Gaussian basis sets for solids made simple, *Journal of Chemical Theory and Computation* **18**, 1595 (2022).
- [36] S. Goedecker, M. Teter, and J. Hutter, Separable dual-space Gaussian pseudopotentials, *Phys. Rev. B* **54**, 1703 (1996).
- [37] C. Hartwigsen, S. Goedecker, and J. Hutter, Relativistic separable dual-space Gaussian pseudopotentials from H to Rn, *Phys. Rev. B* **58**, 3641 (1998).
- [38] M. Marsman, A. Grüneis, J. Paier, and G. Kresse, Second-order Møller–Plesset perturbation theory applied to extended systems. I. Within the projector-augmented-wave formalism using a plane wave basis set, *The Journal of Chemical Physics* **130**, 184103 (2009), https://pubs.aip.org/aip/jcp/article-pdf/doi/10.1063/1.3126249/9452255/184103.1_online.pdf.
- [39] J. J. Shepherd, A. Grüneis, G. H. Booth, G. Kresse, and A. Alavi, Convergence of many-body wave-function expansions using a plane-wave basis: From homogeneous electron gas to solid state systems, *Phys. Rev. B* **86**, 035111 (2012).
- [40] J. Klimeš, M. Kaltak, E. Maggio, and G. Kresse, Singles correlation energy contributions in solids, *The Journal of Chemical Physics* **143**, 102816 (2015).
- [41] W. Kohn, *Phys. Rev. Lett.* **76**, 3168 (1996).
- [42] H. N. Rojas, R. W. Godby, and R. J. Needs, Space-Time Method for *ab initio* Calculations of Self-Energies and Dielectric Response Functions of Solids, *Phys. Rev. Lett.* **74**, 1827 (1995).
- [43] J. K. Klimeš, M. Kaltak, and G. Kresse, Predictive GW calculations using plane waves and pseudopotentials, *Phys. Rev. B* **90**, 075125 (2014).
- [44] I. Y. Zhang, X. Ren, P. Rinke, V. Blum, and M. Scheffler, Numeric atom-centered-orbital basis sets with valence-correlation consistency from H to Ar, *New J. Phys.* **15**, 123033 (2013).
- [45] I. Y. Zhang, A. J. Logsdail, X. Ren, S. V. Levchenko, L. Ghiringhelli, and M. Scheffler, Test set for materials science and engineering with user-friendly graphic tools for error analysis: Systematic benchmark of the numerical and intrinsic errors in state-of-the-art electronic-structure approximations, *New J. Phys.* **21**, 013025 (2019).
- [46] V. Blum, F. Hanke, R. Gehrke, P. Havu, V. Havu, X. Ren, K. Reuter, and M. Scheffler, Ab-initio molecular simulations with numeric atom-centered orbitals, *Comp. Phys. Comm.* **180**, 2175 (2009).
- [47] I. Y. Zhang, X. Ren, P. Rinke, V. Blum, and M. Scheffler, Numeric atom-centered-orbital basis sets with valence-correlation consistency from H to Ar, *New Journal of Physics* **15**, 123033 (2013).
- [48] E. Van Lenthe and E. J. Baerends, Optimized slater-type basis sets for the elements 1–118, *Journal of Computational Chemistry* **24**, 1142 (2003).
- [49] G. t. Te Velde, F. M. Bickelhaupt, E. J. Baerends, C. Fonseca Guerra, S. J. van Gisbergen, J. G. Snijders, and T. Ziegler, Chemistry with ADF, *Journal of Computational Chemistry* **22**, 931 (2001).
- [50] R. C. Raffanetti, Even-tempered atomic orbitals. II. Atomic SCF wavefunctions in terms of even-tempered exponential bases, *J. Chem. Phys.* **59**, 5936 (1973).
- [51] J. A. Nelder and R. Mead, A simplex method for function minimization, *The computer journal* **7**, 308 (1965).
- [52] X. Ren, A. Tkatchenko, P. Rinke, and M. Scheffler, Beyond the Random Phase Approximation for the Electron Correlation Energy: The Importance of Single Excitations, *Phys. Rev. Lett.* **106**, 153003 (2011).
- [53] S. Yang and X. Ren, Phase stability of the argon crystal: first-principles study based on random phase approximation plus renormalized single excitation corrections, *New J. Phys.* **24**, 033049 (2022).
- [54] M. N. Tahir, T. Zhu, H. Shang, J. Li, V. Blum, and X. Ren, Localized resolution of identity approach to the analytical gradients of random-phase approximation ground-state energy: algorithm and benchmarks, *Journal of Chemical Theory and Computation* **18**, 5297 (2022).
- [55] A. Halkier, T. Helgaker, P. Jørgensen, W. Klopper, H. Koch, J. Olsen, and A. K. Wilson, *Chem. Phys. Lett.* **286**, 243 (1998).
- [56] T. Helgaker, W. K. H. Koch, and J. Noga, Basis-set convergence of correlated calculations on water, *J. Chem. Phys.* **106**, 9639 (1997).
- [57] E. van Lenthe, E. Baerends, and J. Snijders, Relativistic total energy using regular approximations, *J. Chem. Phys.* **101**, 9783 (1994).
- [58] A. Togo and I. Tanaka, First principles phonon calculations in materials science, *Scr. Mater.* **108**, 1 (2015).
- [59] L. A. Schwalbe, R. K. Crawford, H. H. Chen, and R. A. Aziz, Thermodynamic consistency of vapor pressure and calorimetric data for argon, krypton, and xenon, *J. Chem. Phys.* **66**, 4493 (1977).
- [60] D. Losee and R. Simmons, Thermal-expansion measurements and thermodynamics of solid krypton, *Phys. Rev.* **172**, 944 (1968).
- [61] K. Rościszewski, B. Paulus, P. Fulde, and H. Stoll, Ab initio coupled-cluster calculations for the fcc and hcp structures of rare-gas solids, *Phys. Rev. B* **62**, 5482 (2000).
- [62] J. P. Perdew, M. Ernzerhof, and K. Burke, Rationale of mixing exact exchange with density functional approximations, *J. Chem. Phys.* **105**, 9982 (1996).
- [63] J. Heyd, G. E. Scuseria, and M. Ernzerhof, Hybrid functionals based on a screened coulomb potential, *J. Chem. Phys.* **118**, 8207 (2003).
- [64] A. Tkatchenko and M. Scheffler, *Phys. Rev. Lett.* **102**, 073005 (2009).
- [65] A. Tkatchenko, R. A. DiStasio Jr., R. Car, and M. Scheffler, *Phys. Rev. Lett.* **108**, 236402 (2012).
- [66] J. Harl and G. Kresse, Cohesive energy curves for noble gas solids calculated by adiabatic connection fluctuation-dissipation theory, *Phys. Rev. B* **77**, 045136 (2008).

- [67] F. Ke, L. Zhang, Y. Chen, K. Yin, C. Wang, Y.-K. Tzeng, Y. Lin, H. Dong, Z. Liu, J. S. Tse, *et al.*, Synthesis of atomically thin hexagonal diamond with compression, *Nano letters* **20**, 5916 (2020).
- [68] A. P. Nayak, S. Bhattacharyya, J. Zhu, J. Liu, X. Wu, T. Pandey, C. Jin, A. K. Singh, D. Akinwande, and J.-F. Lin, Pressure-induced semiconducting to metallic transition in multilayered molybdenum disulphide, *Nature communications* **5**, 3731 (2014).
- [69] Z. Chi, X. Chen, F. Yen, F. Peng, Y. Zhou, J. Zhu, Y. Zhang, X. Liu, C. Lin, S. Chu, *et al.*, Superconductivity in pristine $2H_a$ - MoS₂ at ultrahigh pressure, *Phys. Rev. Lett.* **120**, 037002 (2018).
- [70] A. Jephcoat, H. Mao, L. Finger, D. Cox, and R. Hemley, Pressure-induced structural phase transitions in solid xenon, *Phys. Rev. Lett.* **59**, 2670 (1987).
- [71] H. Cynn, C. S. Yoo, B. Baer, V. Iota-Herbei, A. K. McMahan, M. Nicol, and S. Carlson, Martensitic fcc-to-hcp Transformation Observed in Xenon at High Pressure, *Phys. Rev. Lett.* **86**, 4552 (2001).
- [72] K. A. Goettel, J. H. Eggert, I. F. Silvera, and W. C. Moss, Optical evidence for the metallization of xenon at 132 (5) gpa, *Phys. Rev. Lett.* **62**, 665 (1989).
- [73] D. Errandonea, B. Schwager, R. Boehler, and M. Ross, Phase behavior of krypton and xenon to 50 GPa, *Phys. Rev. B* **65**, 214110 (2002).
- [74] D. Errandonea, R. Boehler, S. Japel, M. Mezouar, and L. R. Benedetti, Structural transformation of compressed solid Ar: An X-ray diffraction study to 114 GPa, *Phys. Rev. B* **73**, 092106 (2006).
- [75] R. Reichlin, K. E. Brister, A. K. McMahan, M. Ross, S. Martin, Y. K. Vohra, and A. L. Ruoff, Evidence for the Insulator-Metal Transition in Xenon from Optical, X-Ray, and Band-Structure Studies to 170 GPa, *Phys. Rev. Lett.* **62**, 669 (1989).
- [76] M. Ross, R. Boehler, and P. Söderlind, Xenon melting curve to 80 GPa and $5p-d$ hybridization, *Phys. Rev. Lett.* **95**, 257801 (2005).
- [77] A. Rosa, G. Garbarino, R. Briggs, V. Svitlyk, G. Morard, M. A. Bouhifd, J. Jacobs, T. Irifune, O. Mathon, and S. Pascarelli, Effect of the fcc-hcp martensitic transition on the equation of state of solid krypton up to 140 GPa, *Phys. Rev. B* **97**, 094115 (2018).
- [78] P. Schwerdtfeger, K. G. Steenbergen, and E. Pahl, Relativistic coupled-cluster and density-functional studies of argon at high pressure, *Phys. Rev. B* **95**, 214116 (2017).
- [79] E. Kim, M. Nicol, H. Cynn, and C.-S. Yoo, Martensitic fcc-to-hcp Transformations in Solid Xenon under Pressure: A First-Principles Study, *Phys. Rev. Lett.* **96**, 035504 (2006).
- [80] I. Kwon, L. A. Collins, J. D. Kress, and N. Troullier, First-principles study of solid Ar and Kr under high compression, *Phys. Rev. B* **52**, 15165 (1995).
- [81] J. K. Dewhurst, R. Ahuja, S. Li, and B. Johansson, Lattice dynamics of solid xenon under pressure, *Phys. Rev. Lett.* **88**, 075504 (2002).
- [82] A. Polian, J. Itie, E. Dartyge, A. Fontaine, and G. Tourillon, X-ray absorption spectroscopy on solid krypton up to 20 GPa, *Phys. Rev. B* **39**, 3369 (1989).
- [83] A. P. Jephcoat, Rare-gas solids in the earth's deep interior, *Nature* **393**, 355 (1998).